applied sciences

MDPI

Article

Experimental Research of the Structure Condition Using Geodetic Methods and Crackmeter

Jacek Sztubecki [1], Szymon Topoliński [1], Maria Mrówczyńska [2,*], Baki Bağrıaçık [3] and Ahmet Beycioğlu [4]

[1] Faculty of Civil and Environmental Engineering and Architecture, University of Science and Technology in Bydgoszcz, 85-796 Bydgoszcz, Poland; jacek.sztubecki@pbs.edu.pl (J.S.); szymon.topolinski@pbs.edu.pl (S.T.)
[2] Faculty of Civil Engineering, Architecture and Environmental Engineering, University of Zielona Góra, 65-417 Zielona Góra, Poland
[3] Department of Civil Engineering, Çukurova University, Adana 01330, Turkey; bbagriacik@cu.edu.tr
[4] Department of Civil Engineering, Adana Alparslan Türkeş Science and Technology University, Adana 01250, Turkey; abeycioglu@atu.edu.tr
* Correspondence: m.mrowczynska@ib.uz.zgora.pl

Abstract: The article presents an approach to monitoring the structure's condition with two measurement methods: the SHM-X crackmeter and the classic geodetic method of determining displacements, supplemented with additional information on the condition of the external environment obtained from thermal images. The study aimed to propose an approach combining geodetic and non-geodetic methods of assessing the condition of a structure and its effectiveness in practical application. The research facility is a public utility building of the Bydgoszcz University of Technology with a reinforced concrete structure. Objects of this type require periodic tests of their constancy. Interpreting the test results and identifying possible dangerous states that may indicate the risk of a construction failure is extremely important. The results presented in the article are an extension of the previous ones, in which several factors that could have a destructive effect on the structure were excluded. Observation of the object showed that only the reinforced construction plate is deformed. The only factor influencing the change in structure geometry is thermal changes. As part of the tests in places where cracks were noticed, the SHM-X crackmeter was used to measure the cracks' opening. In the geodetic research, measurements of the measurement and control network displacement were carried out, in which the TDRA6000 laser station measurement technology was used. The control points were also placed in places where the width of the cracks was directly observed. The proposed approach, with the applied calculation scheme and supplementing the information with the temperature measurement with thermal images, showed the submillimeter accuracy of the determined 3D displacements of the controlled points. Additionally, the parallel application of these methods gives a complete picture of changes in the structure elements, in which signs of destruction appear under the influence of stress.

Keywords: structural health monitoring; displacement surveying; breakdowns of building structures; civil engineering

check for updates

Citation: Sztubecki, J.; Topoliński, S.; Mrówczyńska, M.; Bağrıaçık, B.; Beycioğlu, A. Experimental Research of the Structure Condition Using Geodetic Methods and Crackmeter. *Appl. Sci.* **2022**, *12*, 6754. https://doi.org/10.3390/app12136754

Academic Editors: Yiching Lin and Chia-Chi Cheng

Received: 17 May 2022
Accepted: 1 July 2022
Published: 3 July 2022

Publisher's Note: MDPI stays neutral with regard to jurisdictional claims in published maps and institutional affiliations.

Copyright: © 2022 by the authors. Licensee MDPI, Basel, Switzerland. This article is an open access article distributed under the terms and conditions of the Creative Commons Attribution (CC BY) license (https://creativecommons.org/licenses/by/4.0/).

1. Introduction

Using buildings safely should be subject to obligatory periodic inspections of their technical condition and structure conditions. Such an approach allows for assessing their condition throughout their life cycle, planning the necessary renovation works, and identifying the negative impact of neighboring facilities, biological and chemical co-development, and weather conditions [1–3]. During these inspections, the method of visual construction assessment is used in the first place, which allows for diagnosing only the obvious, visible signs of damage or failure. However, the exact determination of the technical condition of a building requires a series of tests, measurements, and analyses, which may be a complex

and challenging task [4,5]. Therefore, the research process, which supports the assessment of the technical condition of the structure, is supplemented with measurements of displacements and deformations using geodetic and non-geodetic techniques.

The primary symptom of negative phenomena occurring in building objects is their displacements and deformations. Geodetic monitoring is used, among other things, to determine displacements and deformations of engineering structures. It includes measurements, the subsequent analysis of which allows concluding the dynamics of the occurrence of changes in the structure. These measurements also provide information on the geometrical state of objects and changes in time and allow for obtaining additional information, for example, on the object's surface and volume [6–8]. The geodetic monitoring method depends on the object's structure, its location in space, the size and speed of changes, and the geodetic technology that can be used and conditioned by the measurements' cyclical nature [9–11]. The displacements are monitored by performing a measurements series of the measurement network and control points set up in the object, and the structure should be optimized in terms of the possibility of making measurements and the correctness of determining displacements [12–14]. Modern measuring technologies enable the implementation of tasks that have not been possible until now by traditional methods while ensuring the required precision. Currently, construction objects and subsoil can be monitored using classic geodetic methods [14,15], the GNSS system and gravimetric measurements [16–18], unmanned aerial vehicles, and laser scanning [19–21], and supplemented with GIS technology [22,23]. The analytical part of the displacement determination process and the prediction of changes and planning of modernization work on the facilities can also be supported by intelligent monitoring systems based on artificial intelligence [24–27].

The displacements and deformations of elements of engineering structures can be determined using modern laser devices. Today, these technologies are often used in industrial metrological measurements and are characterized by the high precision of distance measurement, up to $+/-$ 15 μm + 6 μm/m when measured per retroreflector and the operating range of 120 m [28,29]. The possibilities of using the coordinate laser station were presented [30]. Cyclical measurements of the structure geometry make it possible to compare its displacements in different periods of use. The correct results' interpretation, together with the assessment of the technical condition of the structure, gives a picture of the actual operation of the monitored facility [31].

An important aspect when measuring and monitoring the behavior of buildings is obtaining data with adequate accuracy in real-time [32]. For this purpose, non-geodetic methods can be used for this purpose, including measurement methods using analog and digital feeler gauges, industrial cameras, laser beam emitting devices, and radar sensors [33–35]. Kot et al., in their article, reviewed the latest achievements in non-destructive research techniques, including sweep frequency approach, ground-penetrating radar, infrared technique, fiber optics sensors, camera-based methods, laser scanner techniques, acoustic emission, and ultrasonic techniques [36]. Teng et al. presented an innovative technique for assessing moisture content and controlling the deterioration of concrete blocks using a smart antenna [37]. Sensor technology also allows for real-time monitoring of the structure's condition (damage of concrete due to corrosion of reinforcement) and the quantity and quality of natural resources. It enables precise monitoring of changes in environmental conditions and the depletion of natural resources over vast areas, which helps minimize the effects of natural disasters and prevent/minimize the serious pollution effects [38,39]. To compare the results obtained with advanced geodetic measurement and calculation methods, it is possible to use a non-complicated method of testing the crack width using the SHM-X crackmeter. In engineering conditions, it is often used by direct measurement of pins with a caliper [40], but it is also possible to measure continuously using electronic sensors and appropriate software [41]. This approach allows for accuracy in obtaining real-time information and verifying the results obtained from geodetic methods.

In long-span building structures, there may be periodic forced states of the structure resulting from a varying temperature gradient. This phenomenon is primarily significant

for steel structures but may also occur in reinforced concrete structures characterized by low stiffness. The influence of temperature on the deformation phenomena of structural elements and entire structures, considering various materials, has been widely described in the literature [42–47]. In recent years, along with new technologies, the temperature measurement of building objects, structural elements, and surroundings has been performed using thermovision [48,49]. These are non-contact methods, using thermal imaging cameras, enabling the simultaneous observation of the temperature distribution on the surface of the tested object, temperature measurement, and its registration in the form of a thermogram [50,51]. Since our previous research excluded the influence of soil factors on the displacement in the discussed object, an attempt was made to determine the changes taking into account the temperature gradient, which was determined on the basis of infrared images.

The study aimed to propose a hybrid approach combining geodetic and non-geodetic methods of assessing the condition of a structure with the assessment of its effectiveness in application to a public utility facility. The article presents the results analysis of the displacement measurements of a building object to achieve the goal. Two measurement methods were used: measurement of absolute displacements using the Leica TDRA6000 coordinate laser station and measurement of the aperture width with the SHM X crackmeter. The results were supplemented by additional information using thermal images taken during measurements with a camera FLIR SC660 thermal imaging machine. The obtained results made it possible to formulate conclusions regarding the change in the geometry of the structure of a public utility facility. These changes cause visible scratches on the walls inside the building. The rest of the article is organized as follows: Section 2 describes the test object. Section 3 presents methods for solving the problem to determine the vertical displacements of the measurement and control network points. Section 4 presents the research results and the discussion of the obtained results. Finally, Section 5 contains conclusions and key findings and shows future directions for work.

2. Case Study

The analyzed object is an above-ground passage with a light reinforced concrete structure characterized by low stiffness due to its slenderness. The location of the object under study is presented in Figure 1. The beams with the bottom plate, pillars, and roof beams form a spatial skeleton. A checkered brick was used as the filling of the supporting skeleton. The structure is supported by 12 pillars. The foundation footings of the pillars are made of reinforced concrete, monolithic, common to every two adjacent columns. They are located at different depths: about 4.0 m below the sea level from the south (directly next to the Auditorium Novum building); 1.95 m below ground level on the north side, at building 2.1 and 1.70 m below ground level for the four middle columns [52,53]. There are expansive soils at the foundation level of the footing: clays locally interlayered with silt, lying from 0.5 to 1.5 m below ground level.

The university building is included in the geodetic and non-geodetic monitoring program to create a comprehensive database of the technical condition of the structure. Initially, geodetic monitoring determined vertical displacements of the supports and vertical and horizontal displacements of the fundamental above-ground part of the structure. It is dictated by the fact that there has been increasing damage in the tested structure for over a dozen years, despite the renovation. Initially, the causes were seen in geotechnical conditions, mainly in the possible movements of the expansive subsoil. It should be noted that the monitored facility is located in the zone of Mio-Pliocene Poznań Serie clays. They are the cause of many construction failures in Bydgoszcz [54,55]. However, these assumptions were not confirmed. Several years of observations proved the clay moisture stabilization in the passage foundation [56,57].



Figure 1. Location of the research structure [own elaboration].

3. Materials and Methods

Periodic measurements of displacements were carried out in various weather conditions (season, thermal conditions) at the points of the measurement and control network installed inside the above-ground passage that serves as a communication link between the buildings of the Bydgoszcz University of Technology. The measurement dates and the averaged thermal conditions during the measurements are given in Table 1.

Table 1. Geodetic measurements conditions.

Meas. No.	Date	Construction Temperature
0	2020.07.28	31 °C
1	2020.08.07	35 °C
2	2020.11.04	8 °C
3	2020.12.02	−3 °C

The control points and reference points have been marked inside the passage and on the structure of neighboring buildings in the form of pads glued to the floor (Figure 2). The diagram of the location of the measurement and control network points on the monitored object is presented in Figure 3.



Figure 2. Leica TDRA6000 measuring device and method of stabilizing network points [own analysis].

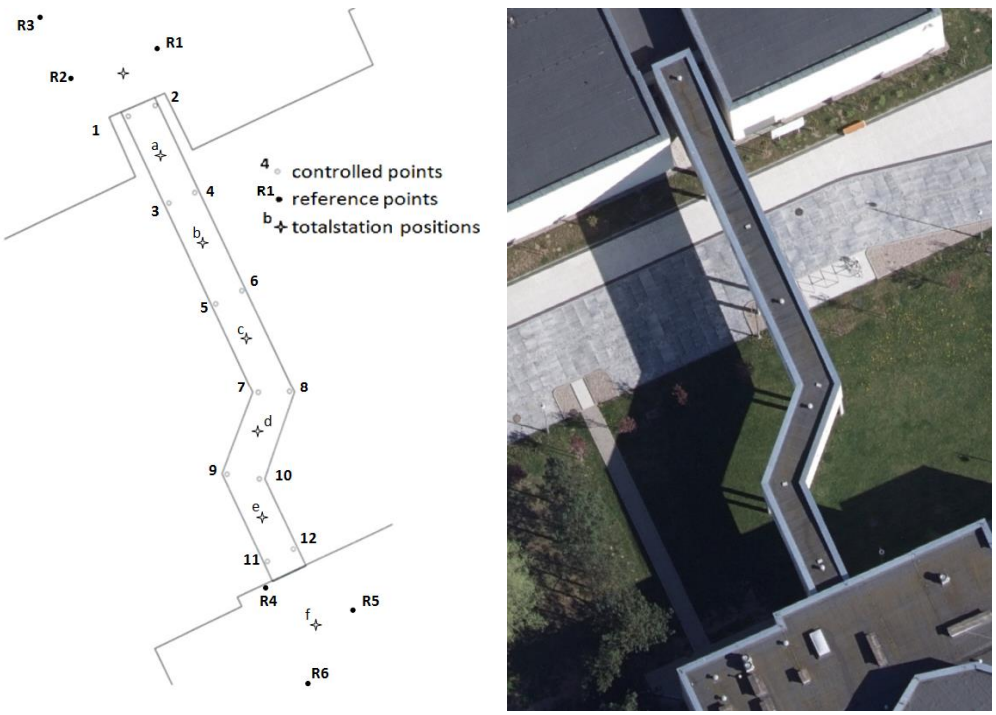

Figure 3. The scheme of the network points distribution [own analysis].

The displacement of the controlled points network was measured with the TDRA6000 laser station (Figure 2). The station is equipped with direct drive technology, which allows obtaining the accuracy of 3D point measurement at the level of 0.25 mm and allows for the observation of horizontal and vertical directions with an average error of 0.0013 g and a distance of 0.2 mm [58,59]. Due to the possible measurement accuracy, the device with appropriate software is an excellent tool for monitoring the condition of engineering structures.

Measurement of the measurement and control network with a laser station consisted of recording the 3D coordinates of the control points at each of the seven free positions. Only the closest control points were observed from each position: the extreme positions—5 points, and the remaining positions—4. Measurements on each position were carried out twice. The calculations were carried out in two stages. In the first stage, the differences in height between the network points were calculated, and then its strict alignment was performed [60–62]. The second stage included determining the assumed network's horizontal displacements. The calculations were made using the plane coordinates (X, Y) of the controlled points at this stage. The calculations were carried out using the isometric transformation integrating the free positions and the Helmert transformation on six reference points (R1–R6), presenting the coordinates of the controlled points from individual measurement series in a uniform local coordinate system. The horizontal displacements of the points were determined by calculating the coordinate differences (X, Y) between the measurement series.

At the same time, displacements were also tested with a crackmeter. The SHM-X crackmeter is a simple tool for measuring changes in crack and expansion joint widths. Four pins (measurement points) are installed at the measuring point, allowing for precise crack control. In expert measurement, displacements in two directions (perpendicular and parallel to the crack) are determined, and a crack or dilatation separates the angle of rotation between the parts of the structure. For a complete analysis, five measurements *P1–P5* of the distance between the selected pins are required [63]. A diagram of the location of measuring points A, B, and C is shown in Figure 4.

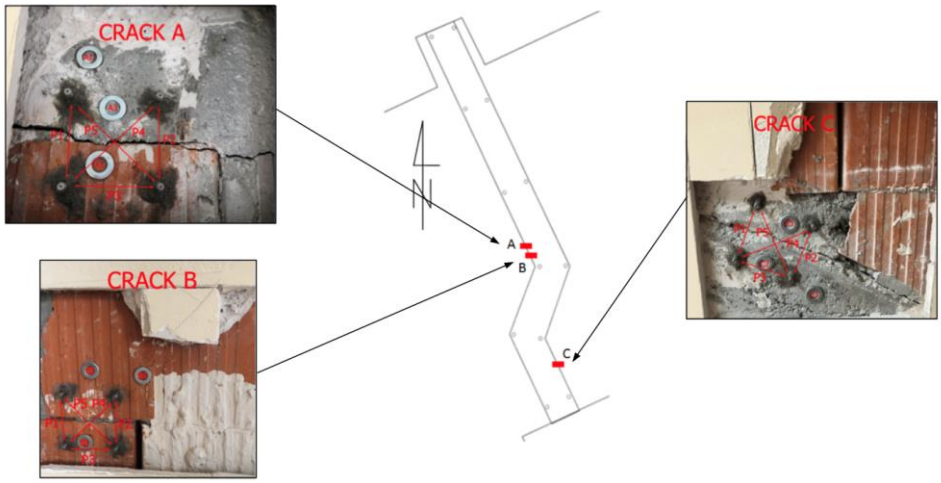

Figure 4. The scheme of the crackmeter location [own analysis].

The essence of the method is to determine the Cartesian coordinates X, Y, and measurement points 1 and 2 concerning points 3 and 4. It was assumed that points 3 and 4 have a fixed position and determine the coordinate system. The origin of the coordinate system is at point 3. Measurement started by selecting the zero measures for which the coordinates were determined of the measurement point 1 (x_1, y_1) and 2 (x_2, y_2) and the initial angle (α_0). For subsequent measurements, we determined the desired displacements of points 1 (Δx_1, Δy_1) and 2 (Δx_2, Δy_2) and the angle of rotation (α). The scheme adopted for the measurements and determination of the coordinates is shown in Figure 5.

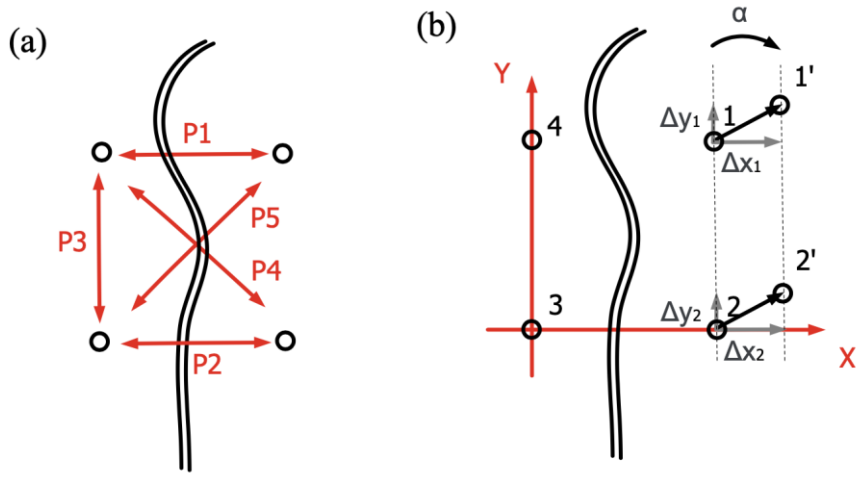

Figure 5. The SHM crackmeter measurement method (own study based on [64]): (**a**) complete analysis measurement, (**b**) coordinates calculating method.

The zero (initial) coordinates of the measurement pins 1 and 2 are determined based on the system of circle equations, where the general equation of the circle is as follows:

$$(x-a)^2 + (y-b)^2 = r^2 \tag{1}$$

where:

$S = (a, b)$—circle center,

r—circle radius.

Each coordinate is determined by finding the intersection of two circles whose diameters for points 1 and 2 are the distances (Figure 5b) $P1$ and $P5$ and $P2$ and $P4$. After transformations and taking into account the accuracy of 0.01 mm and the pin diameter ∅, the formulas for the coordinates of measurement pins 1 and 2 (2–5) finally take the form:

$$x_1 = \sqrt{\left((P5-\varnothing)^2 - \left(\frac{\left((P5-\varnothing)^2 - (P1-\varnothing)^2 + (P3-\varnothing)^2\right)^2}{2\times(P3-\varnothing)}\right)\right)} \tag{2}$$

$$y_1 = \frac{(P5-\varnothing)^2 - (P1-\varnothing)^2 + (P3-\varnothing)^2}{2\times(P3-\varnothing)} \tag{3}$$

$$x_2 = \sqrt{\left((P2-\varnothing)^2 - \left(\frac{\left((P2-\varnothing)^2 - (P4-\varnothing)^2 + (P3-\varnothing)^2\right)^2}{2\times(P3-\varnothing)}\right)\right)} \tag{4}$$

$$y_2 = \frac{(P2-\varnothing)^2 - (P4-\varnothing)^2 + (P3-\varnothing)^2}{2\times(P3-\varnothing)} \tag{5}$$

where:

$P1$–$P5$—measured distances between pins

x_2, y_2—points 1 and 2 coordinates,

Δx_1, Δy_1—point 1 and 2 displacements,

α—rotation angle,

$\varnothing$—pin diameter.

The formula for the initial angle α_0 (6), taking into account the accuracy of the measurement and rounding, takes the value:

$$\alpha_0 = \operatorname{atan}\frac{(x_1 - x_2)}{(y_1 - y_2)} \tag{6}$$

The formulas for the relative displacements of pins 1 and 2 (7–10) are obtained by redetermining the coordinates and subtracting the appropriate starting coordinates from them [65]:

$$\Delta x_1 = \sqrt{\left((P5 - \varnothing)^2 - \left(\frac{\left((P5 - \varnothing)^2 - (P1 - \varnothing)^2 + (P3 - \varnothing)^2\right)^2}{2 \times (P3 - \varnothing)}\right)\right)} - x_1 \tag{7}$$

$$\Delta y_1 = \frac{(P5 - \varnothing)^2 - (P1 - \varnothing)^2 + (P3 - \varnothing)^2}{2 \times (P3 - \varnothing)} - y_1 \tag{8}$$

$$\Delta x_2 = \sqrt{\left((P2 - \varnothing)^2 - \left(\frac{\left((P2 - \varnothing)^2 - (P4 - \varnothing)^2 + (P3 - \varnothing)^2\right)^2}{2 \times (P3 - \varnothing)}\right)\right)} - x_2 \tag{9}$$

$$\Delta y_2 = \frac{(P2 - \varnothing)^2 - (P4 - \varnothing)^2 + (P3 - \varnothing)^2}{2 \times (P3 - \varnothing)} - y_2 \tag{10}$$

The change in the angle of rotation α (11) is determined by taking into account the displacements of the pins during subsequent measurements and subtracting the initial angle of rotation [65].

$$\alpha = \operatorname{atan}\frac{(\Delta x_1 + x_1) - (\Delta x_2 + x_2)}{(\Delta y_1 + y_1) - (\Delta y_2 + y_2)} - \alpha_0 \tag{11}$$

4. Results and Discussion

As shown in Table 1, four series of measurements were carried out for determining the displacements of the controlled points in the network: measure 0—2020.07.28, measurement 1—2020.08.07, measurement 2—2020.11.04, and measurement 3—2020.12.02, which were characterized by variables temperature conditions.

The temperature was read from the infrared images using the FLIR TOOLS software. Below is a detailed summary of the structure thermic observed for each measurement series (Table 2). Points T1, T2, T3, and T7 are on the external walls, while points T4, T5, T6, and T8 are on the internal walls. The location of the points for which the temperature was read is shown in Figure 6.

Table 2. Construction thermal overview.

Point No.	Construction Temperature (°C)			
	2020.07.28	2020.08.07	2020.11.04	2020.12.02
T1	33.0	36.5	6.9	−3.4
T2	32.7	36.4	7.1	−3.2
T3	35.7	44.3	7.7	−3.0
T4	27.3	26.7	17.6	13.2
T5	27.9	27.5	17.7	12.9
T6	27.5	27.0	17.9	13.4
T7	32.0	34.5	8.0	−2.6
T8	26.1	25.2	17.4	12.0

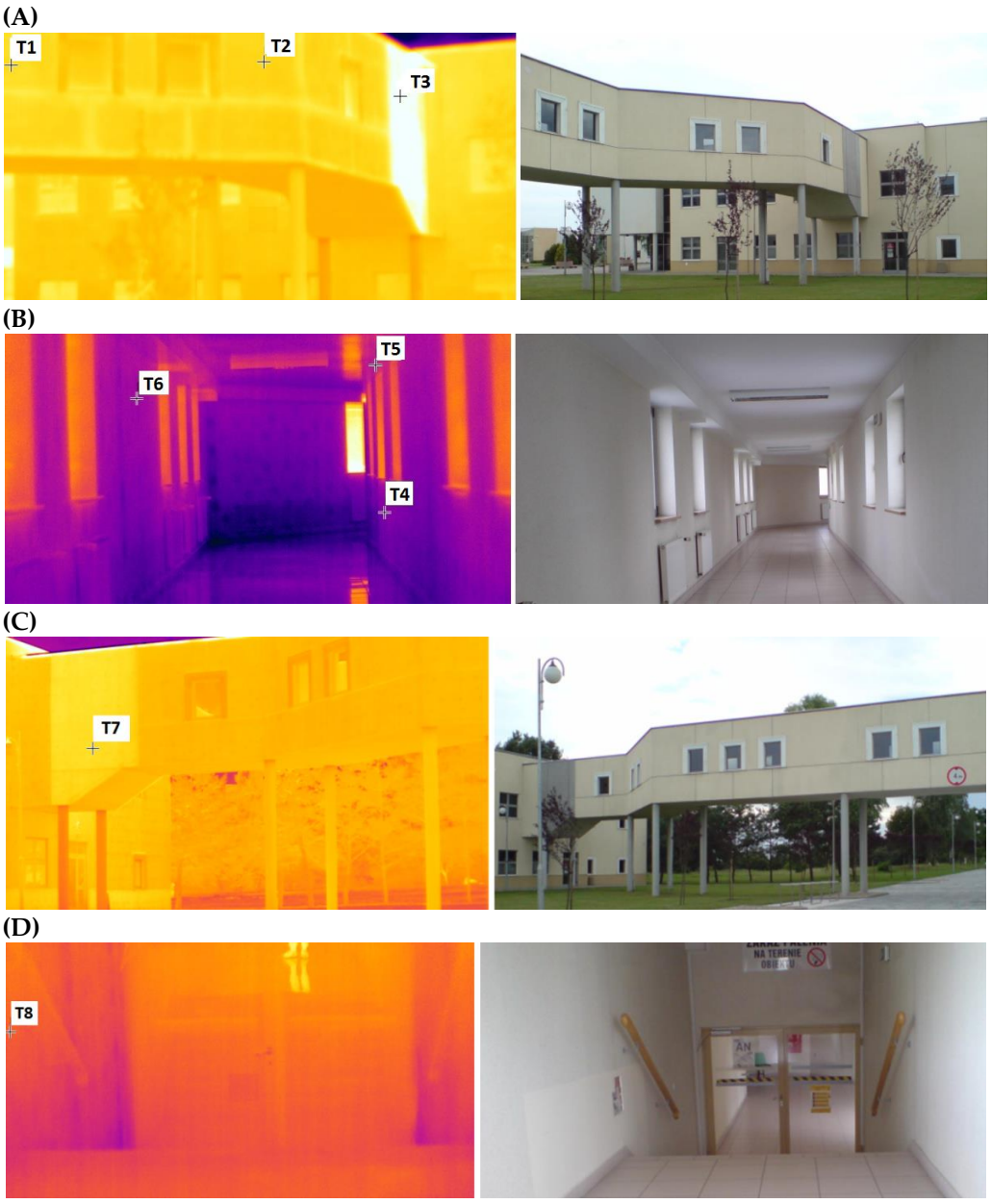

Figure 6. Point temperature distribution. (**A**) The location of the structure's external points for which the temperature was read. (**B**) The location of the structure's internal points for which the temperature was read. (**C**) The location of the structure's external points for which the temperature was read. (**D**) The location of the structure's internal points for which the temperature was read.

Based on geodetic measurements, it was possible to determine the horizontal and vertical displacements of the controlled points. The values of the determined vertical displacements (dZ) and their mean errors (m_{dZ}) are summarized in Table 3.

Table 3. The values of vertical displacements and their mean errors.

Point No.	Meas. 0–Meas. 1		Meas. 0–Meas. 2		Meas. 0–Meas. 3	
	dZ (mm)	m_{dZ} (mm)	dZ (mm)	m_{dZ} (mm)	dZ (mm)	m_{dZ} (mm)
1	0.05	0.02	−0.08	0.08	−0.23	0.07
2	0.07	0.02	−0.03	0.08	−0.31	0.07
3	0.47	0.02	−0.70	0.08	−1.56	0.07
4	0.36	0.02	−0.94	0.08	−1.66	0.07
5	0.52	0.03	−0.80	0.08	−1.43	0.08
6	0.32	0.03	−0.87	0.08	−1.50	0.08
7	0.33	0.03	−0.80	0.08	−1.20	0.08
8	0.22	0.03	−0.73	0.08	−1.15	0.08
9	0.33	0.02	−0.61	0.08	−1.21	0.07
10	0.21	0.02	−0.58	0.08	−1.18	0.07
11	0.16	0.02	−0.52	0.08	−0.97	0.07
12	0.12	0.02	−0.61	0.08	−1.02	0.07

Using the transformation methods: isometric and Helmert, the horizontal displacements of the network control points were determined [57,58]. The displacement values are shown in Table 4.

Table 4. Determined horizontal displacements values.

Point No.	Meas. 0–Meas. 1		Meas. 0–Meas. 2		Meas. 0–Meas. 3	
	dX (mm)	dY (mm)	dX (mm)	dY (mm)	dX (mm)	dY (mm)
1	0.16	0.33	0.85	0.90	1.42	0.67
2	0.17	0.31	0.86	0.69	1.33	0.42
3	0.36	1.01	0.66	1.69	0.87	1.08
4	0.17	1.02	0.39	1.59	0.70	0.92
5	0.29	1.95	−0.05	2.29	−0.60	2.40
6	0.11	1.91	−0.31	2.21	−0.81	2.19
7	0.29	2.39	−0.70	2.78	−2.00	3.20
8	0.08	2.53	−1.07	2.82	−2.39	3.04
9	−0.15	2.13	−1.41	2.84	−2.96	3.54
10	−0.05	1.94	−1.41	2.71	−2.87	3.19
11	−0.37	0.41	−2.46	1.28	−4.42	1.49
12	0.08	0.51	−1.88	1.35	−3.91	1.46

The analysis of the determining horizontal displacements accuracy in the first phase of calculations was based on the isomorphic transformation error determination for each station of the laser station. The values of these errors are presented in Table 5.

Table 5. Isometric transformation errors (mm).

Station No.	Transformation Error (mm)			
	Meas. 0	Meas. 1	Meas. 2	Meas. 3
S1	0.11	0.12	0.16	0.10
S2	0.08	0.23	0.10	0.16
S3	0.12	0.22	0.10	0.22
S4	0.16	0.14	0.21	0.09
S5	0.22	0.13	0.12	0.09
S6	0.08	0.06	0.27	0.23
S7	0.13	0.15	0.08	0.14

After merging the positions, starting from the second measurement series, using the reference points (R1–R6), the network points were transformed into the system from the

output measurement (Measurement 0). For this purpose, the Helmert transformation was used. The values of the transformation errors are shown in the Table 6.

Table 6. Helmert transformation errors (mm).

Meas. 0–Meas. 1	Meas. 0–Meas. 2	Meas. 0–Meas. 3
0.82	0.61	0.55

The vertical and horizontal displacements determined with the crackmeter are shown in Table 7, Table 8, and Table 9, respectively, for cracks A, B, and C (Figure 4).

Table 7. Crack A measurement results.

Meas No.	***Zero* Measurement**				
	Measuring points Coordinates				***Zero* Angle**
	x_1	y_1	x_2	y_2	α_0 (°)
0	71.90	74.42	73.11	0.31	−0.94
Meas. No.	**Measurement results**				
	Measuring points displacements				**Rotation**
	Δx_1 [mm]	Δy_1 [mm]	Δx_2 [mm]	Δy_2 [mm]	α [°]
1	−0.04	0.03	−0.03	0.03	−0.01
2	−0.12	−0.09	−0.07	0.02	−0.04
3	−0.07	0.04	−0.02	0.04	−0.04

Table 8. Crack B measurement results.

Meas. No.	***Zero* Measurement**				
	Measuring Points Coordinates				***Zero* Angle**
	x_1	y_1	x_2	y_2	α_0 (°)
0	74.03	73.33	73.63	−1.94	0.30
Meas. No.	**Measurement results**				
	Measuring points displacements				**Rotation**
	Δx_1 (mm)	Δy_1 (mm)	Δx_2 (mm)	Δy_2 (mm)	α (°)
1	−0.05	−0.01	0.03	0.12	−0.06
2	−0.05	0.00	0.02	0.19	−0.05
3	−0.08	0.03	0.05	0.14	−0.10

Table 9. Crack C measurement results.

Meas. No.	***Zero* Measurement**				
	Measuring points Coordinates				***Zero* Angle**
	x_1	y_1	x_2	y_2	α_0 (°)
0	73.97	74.66	74.28	−0.59	−0.24
Meas. No.	**Measurement results**				
	Measuring points displacements				**Rotation**
	Δx_1 (mm)	Δy_1 (mm)	Δx_2 (mm)	Δy_2 (mm)	α (°)
1	0.02	−0.06	−0.07	0.02	0.07
2	0.08	−0.02	−0.04	0.17	0.09
3	0.08	−0.03	−0.08	0.10	0.12

Due to the frequent displacements caused by swelling or shrinking, subsoils are usually the first cause of failure, especially in areas with expansive soil (as is the case in the area where the monitored facility is located). This is especially true for lightweight structures that exert little pressure on the subsoil. However, after a series of tests, it was found that the destruction reason of the object is most likely changes in its geometry caused by its periodic thermal changes, and the displacements of the subsoil do not affect the structure. The main reason turned out to be, first of all, the thermal expansion of the structure. During the research, the maximum value of vertical displacements was −1.66 mm for point no. 3, with the temperature difference between the initial measurement (Measurement 0) 0 and the current measurement (Measurement 3) equaling 33 °C. Furthermore, changes in the horizontal plane were the largest for the same period, and the maximum for the *X*-axis was −4.42 mm for point no.11, and the *Y*-axis + 3.54 mm for point no. 9. B and C also in the Measurement 0–Measurement 3-period additionally, the torsion angle α was then the maximum and amounted to -0.10° and 0.12°, respectively, for points B and C.

The research shows the importance of comprehensive monitoring of the structure and individual approach to each case at the initial stage [66]. Furthermore, carrying out measurement campaigns on construction objects and a wider perspective is important from the point of view of the acquired values and the assessment of the entire measurement structure stability [67]. A similar use of the series of geodetic and non-decision observations in the form of regular measurement campaigns was proposed by: low-accuracy measurements integrated by GPS, and theodolite observations for the displacement horizon allow identifying the expected settlement process caused by the weight of the structure acting on compressible soils at the foundation [13,68]. Therefore, the current trends in monitoring areas and buildings aim to combine data obtained from various sources, which was also presented in this article.

5. Conclusions

The geodetic observations of the object indicate that it changes its geometry under the influence of seasonal thermal changes. After excluding geotechnical reasons, the only factor influencing the change in geometry are changes in thermal expansion, by a considerable length, of the reinforced concrete slab. This change is visible in the horizontal direction, where the displacements in the annual cycle are higher than 4 mm. The deformations are not transferred to the other structural elements of the object. Both the pillars and the walls of the building are practically not deformed. Crack openings determined by both measurement methods are insignificant. However, they show a convergence of increasing their size by the values of the obtained horizontal and vertical displacements. This dependence confirms that combining geodetic data with data obtained by other methods allows for the analysis of object changes in a broader aspect and increases the credibility of the engineering interpretation of the measurement results. The geodetic monitoring carried out at the construction site will be continued. Due to the safety of a public facility, it is necessary to identify conditions that may indicate threats to the security of the structure. In future research, it is also planned to extend the traditional measurements (supplemented with thermograms and measures of the width of the identified cracks) with data in the form of a point cloud obtained by laser scanning methods.

Author Contributions: Conceptualization, J.S., S.T., M.M., B.B. and A.B.; methodology, J.S. and S.T.; validation, J.S., S.T. and M.M.; formal analysis, J.S., S.T. and M.M.; data curation, J.S. and S.T.; writing—original draft preparation, J.S., S.T., M.M., B.B. and A.B.; writing—review and editing, J.S., S.T., M.M., B.B. and A.B.; visualization, J.S. and S.T.; supervision, M.M., B.B. and A.B.; project administration, J.S. and S.T. All authors have read and agreed to the published version of the manuscript.

Funding: This article/material was supported by the Polish National Agency for Academic Exchange under Grant No. PPI/APM/2019/1/00003.

Institutional Review Board Statement: Not applicable.

Informed Consent Statement: Not applicable.

Data Availability Statement: Not applicable.

Conflicts of Interest: The authors declare no conflict of interest.

References

1. Lengyel, G. Discrete element analysis of gothic masonry vaults for self-weight and horizontal support displacement. *Eng. Struct.* **2017**, *148*, 195–209. [CrossRef]
2. Błaszczak-Bąk, W.; Suchocki, C.; Janicka, J.; Dumalski, A.; Duchnowski, R.; Sobieraj-Żłobińska, A. Automatic Threat Detection for Historic Buildings in Dark Places Based on the Modified OptD Method. *ISPRS Int. J. Geo-Inf.* **2020**, *9*, 123. [CrossRef]
3. Nowogońska, B.; Nowogoński, I. Method of Planning Repairs of the Installation including Building Waste. *Appl. Sci.* **2022**, *12*, 4520. [CrossRef]
4. Catbas, F.N.; Kijewski-Korea, T.; Aktan, A.E. *Structural Identification of Constructed Systems*; American Society of Civil Engineers: Reston, VA, USA, 2013.
5. Karbhari, V.M.; Ansari, F. *Structural Health Monitoring of Civil Infrastructure Systems*; Woodhead Publishing: Cambridge, UK, 2009.
6. Kadaj, R. *Modele, Metody i Algorytmy Obliczeniowe Sieci Kinematycznych w Geodezyjnych Pomiarach Przemieszczeń i Odkształceń Obiektów*; Wydawnictwo Akademii Rolniczej: Kraków, Poland, 1998.
7. Nikulishyn, V.; Savchyn, I.; Lompas, O.; Lozynskyi, V. Applying of geodetic methods for monitoring the effects of waste-slide at Lviv municipal solid waste landfill. *Environ. Nanotechnol. Monit. Manag.* **2020**, *13*, 100291. [CrossRef]
8. Skrzypczak, I.; Kokoszka, W.; Kogut, J.; Oleniacz, G. Methods of Measuring and Mapping of Landslide Areas. *IOP Conf. Ser. Earth Environ. Sci.* **2017**, *95*, 022013. [CrossRef]
9. Zhou, J.; Xiao, H.; Jiang, W.; Bai, W.; Liu, G. Automatic subway tunnel displacement monitoring using robotic total station. *Measurement* **2020**, *15*, 107251. [CrossRef]
10. Donggun, K.; Younghak, K.; Hoon, S. Accelerated cable-stayed bridge construction using terrestrial laser scanning. *Autom. Constr.* **2020**, *117*, 103269. [CrossRef]
11. Gołuch, P.; Kuchmister, J.; Ćmielewski, K.; Bryś, H. Multi-sensors measuring system for geodetic monitoring of elevator guide rails. *Measurement* **2018**, *130*, 18–31. [CrossRef]
12. Mrówczyńska, M.; Sztubecki, J. The network structure evolutionary optimization to geodetic monitoring in the aspect of information entropy. *Measurement* **2021**, *179*, 109369. [CrossRef]
13. Marsella, M.; Nardinocchi, C.; Paoli, A.; Tini, M.A.; Vittuari, L.; Zanutta, A. Geodetic measurements to control a large research infrastructure: The Virgo detector at the European Gravitational Observatory. *Measurement* **2020**, *151*, 107154. [CrossRef]
14. Bryn, M.J.; Afonin, D.A.; Bogomolova, N.N. Geodetic Monitoring of Deformation of Building Surrounding an Underground Construction. *Procedia Eng.* **2017**, *189*, 386–392. [CrossRef]
15. Kurnatowski, M. Test of vibrations influence on the measurement accuracy in the precise digital leveller Trimble Dini 03 and comparison of its vibration sensitivity with leveller NI 002. *Civ. Environ. Eng. Rep.* **2020**, *4*, 111–124. [CrossRef]
16. Przyborski, M.; Pyrchla, J.; Pyrchla, K.; Szulwic, J. Microgal gravity measurements with mgs-6 micro-g lacoste gravimeter. *Sensors* **2019**, *19*, 2592. [CrossRef]
17. Hohensinn, R.; Häberling, S.; Geiger, A. Dynamic displacements from high-rate GNSS: Error modeling and vibration detection. *Measurement* **2020**, *157*, 107655. [CrossRef]
18. Montuori, A.; Anderlini, L.; Palano, M.; Albano, M.; Pezzo, G.; Antoncecchi, I.; Chiarabba, C.; Serpelloni, E.; Stramondo, S. Application and analysis of geodetic protocols for monitoring subsidence phenomena along on-shore hydrocarbon reservoirs. *Int. J. Appl. Earth Obs. Geoinf.* **2018**, *69*, 13–26. [CrossRef]
19. Zaczek-Peplinska, J.; Osińska-Skotak, K. Concrete surface evaluation based on the reflected T.L.S. laser beam's intensity image classification. *Studia Geotech. Mech.* **2018**, *40*, 56–64. [CrossRef]
20. Wójcik, A.; Klapa, P.; Mitka, B.; Piech, I. The use of T.L.S. and UAV methods for measurement of the repose angle of granular materials in terrain conditions. *Measurement* **2019**, *146*, 780–791. [CrossRef]
21. Skrzypczak, I.; Oleniacz, G.; Leśniak, A.; Zima, K.; Mrówczyńska, M.; Kazak, J.K. Scan-to-BIM method in construction: Assessment of the 3D buildings model accuracy in terms inventory measurements. *Build. Res. Inf.* **2022**, 2011703. [CrossRef]
22. Juszczyk, M.; Leśniak, A. Modelling Construction Site Cost Index Based on Neural Network Ensembles. *Symmetry* **2019**, *11*, 411. [CrossRef]
23. Shevchuk, V.; Burshtynska, K.; Korolik, I.; Halochkin, M. Monitoring of horizontal displacements and changes of the riverine area of the Dniester River. *J. Water Land Dev.* **2021**, *49*, 1–15. [CrossRef]
24. Oh, B.K.; Kim, K.J.; Kim, Y.; Park, H.S.; Adeli, H. Evolutionary learning based sustainable strain sensing model for structural health monitoring of high-rise buildings. *Appl. Soft Comput.* **2017**, *58*, 576–585. [CrossRef]
25. Tran-Ngoc, H.; Khatir, S.; De Roeck, G.; Bui-Tien, T.; Abdel Wahab, M. An efficient artificial neural network for damage detection in bridges and beam-like structures by improving training parameters using cuckoo search algorithm. *Eng. Struct.* **2019**, *199*, 109637. [CrossRef]
26. Li, M.; Li, M.; Rem, Q.; Li, H.; Song, L. DRLSTM: A dual-stage deep learning approach driven by raw monitoring data for dam displacement prediction. *Adv. Eng. Inform.* **2022**, *51*, 101510. [CrossRef]

27. Sorkhabi, O.M.; Alizadeh, S.M.S.; Shahdost, F.T.; Heravi, H.M. Deep learning of G.P.S. geodetic velocity. *J. Asian Earth Sci.* **2022**, *7*, 100095. [CrossRef]
28. Wojcik, G.J.; Lakanen, S.A. Laser Tracker, a handy tool for metrology and alignment. In Proceedings of the 7th International Workshops on Accelerator Alignment, Mikazuki, Japan, 11–14 November 2002.
29. Golparvar-Fard, M.; Bohn, J.; Teizer, J.; Savarese, S.; Peña-Mora, F. Evaluation of image-based modeling and laser scanning accuracy for emerging automated performance monitoring techniques. *Autom. Constr.* **2011**, *20*, 1143–1155. [CrossRef]
30. Sztubecki, J.; Mrówczyńska, M.; Bujarkiewicz, A. Proposition of determination of displacements using the TDRA 6000 laser station. *E3S Web Conf.* **2018**, *55*, 00011. [CrossRef]
31. Loschetter, A.; Rohmer, J.; Raucoules, D.; de Michele, M. Sizing a geodetic network for risk-oriented monitoring of surface deformations induced by CO2 injection: Experience feedback with InSAR data collected at In-Salah, Algeria. *Int. J. Greenh. Gas Control* **2015**, *42*, 571–582. [CrossRef]
32. Zeng, Z.P.; Wu, Z.P.; Luo, J.; Yin, H.T.; Li, P.; Tu, Q.M. An analytical calculation method for displacement and force on continuous welded rails in temperature-transition zone. *Constr. Build. Mater.* **2019**, *207*, 228–237. [CrossRef]
33. Zhang, L.; Wei, J. Measurement and control method of clearance between wind turbine tower and blade-tip based on millimeter-wave radar sensor. *Mech. Syst. Signal Process.* **2021**, *149*, 107319. [CrossRef]
34. Kovačič, B.; Kamnik, R.; Solovev, V.; Vatin, N. The Comparison of Measuring and Computing Results of Construction Vertical Displacement. *Procedia Eng.* **2016**, *165*, 926–935. [CrossRef]
35. Serrano-Juan, A.; Vázquez-Suñè, E.; Monserrat, O.; Crosetto, M.; Hoffmann, C.; Ledesma, A.; Criollo, R.; Pujades, E.; Velasco, V.; Garcia-Gil, A.; et al. Gb-SAR interferometry displacement measurements during dewatering in construction works. Case of La Sagrera railway station in Barcelona, Spain. *Eng. Geol.* **2016**, *205*, 104–115. [CrossRef]
36. Kot, P.; Muradov, M.; Gkantou, M.; Kamaris, G.S.; Hashim, K.; Yeboah, D. Recent Advancements in Non-Destructive Testing Techniques for Structural Health Monitoring. *Appl. Sci.* **2021**, *11*, 2750. [CrossRef]
37. Teng, K.H.; Kot, P.; Muradov, M.; Shaw, A.; Hashim, K.; Gkantou, M.; Al-Shamma'a, A. Embedded Smart Antenna for Non-Destructive Testing and Evaluation (NDT&E) of Moisture Content and Deterioration in Concrete. *Sensors* **2019**, *19*, 547. [CrossRef]
38. Kot, P.; Khalid, S.; Hashim, K.S.; Muradov, M.; Al-Khaddar, R. Chapter 17 How can sensors be used for sustainability improvement? In *Methods in Sustainability Science*; Ren, J., Ed.; Elsevier: Amsterdam, The Netherlands, 2021; pp. 321–344. [CrossRef]
39. Omer, G.; Kot, P.; Atherton, W.; Muradov, M.; Gkantou, M.; Shaw, A.; Riley, M.; Hashim, K.; Al-Shamma'a, A. A non-destructive electromagnetic sensing technique to determine chloride level in maritime concrete. *Karbala Int. J. Mod. Sci.* **2021**, *7*, 8. [CrossRef]
40. Drobiec, Ł. Naprawa rys i wzmocnienia murowanych ścian. Cz. 1. Prace poprzedzające naprawę i przemurowanie. *Izolacje* **2017**, *11*, 78–86.
41. Bednarski, Ł.; Sieńko, R.; Howiacki, T. Supporting historical structures technical condition assessment by monitoring of selected physical quantities. *Procedia Eng.* **2017**, *195*, 32–39. [CrossRef]
42. Zhou, M.; Fan, J.S.; Liu, Y.F.; Zhang, J.X.; Duan, X.J.; Lei, S.S. Non-uniform temperature field and effect on construction of large-span steel structures. *Autom. Constr.* **2020**, *119*, 103339. [CrossRef]
43. Wang, Z.; Zhang, N.; Wang, S. Geometry control of special-shaped arch pylon considering seasonal temperature changes during construction. *Structures* **2022**, *36*, 416–427. [CrossRef]
44. Li, M.; Si, W.; Du, S.; Zhang, M.; Ren, Q.; Shen, Y. Thermal deformation coordination analysis of CC-RCC combined dam structure during construction and operation periods. *Eng. Struct.* **2020**, *213*, 110587. [CrossRef]
45. Xu, W.; Chen, D.; Qian, H.; Chen, W. Non-uniform temperature field and effects of large-span spatial truss structure under construction: Field monitoring and numerical analysis. *Structures* **2021**, *29*, 416–426. [CrossRef]
46. Baas, E.J.; Riggio, M.; Barbosa, A.R. Structural health monitoring data collected during construction of a mass-timber building with a data platform for analysis. *Data Brief* **2021**, *35*, 106845. [CrossRef]
47. Zeng, L.; Shu, W.; Liu, Z.; Zou, X.; Wang, S.; Xia, J.; Xu, C.; Xiong, D.; Yang, Z. Vision-based high-precision intelligent monitoring for shield tail clearance. *Autom. Constr.* **2022**, *134*, 104088. [CrossRef]
48. Paraschiv, L.S.; Acomi, N.; Serban, A.; Paraschiv, S. A web application for analysis of heat transfer through building walls and calculation of optimal insulation thickness. *Energy Rep.* **2020**, *6*, 343–353. [CrossRef]
49. Sedighi, A.R.; Kafiri, A.; Sehhati, M.R.; Behdad, F. Life estimation of distribution transformers using thermography: A case study. *Measurement* **2020**, *149*, 106994. [CrossRef]
50. Jakubek, B.; Grochalski, K.; Rukat, W.; Sokol, H. Thermovision measurements of rolling bearings. *Measurement* **2021**, *189*, 115012. [CrossRef]
51. Usamentiaga, R.; Venegas, P.; Guerediaga, J.; Vega, L.; Molleda, J.; Bulnes, F.G. Infrared Thermography for Temperature Measurement and Non-Destructive Testing. *Sensors* **2014**, *14*, 12305–12348. [CrossRef]
52. Kaliskiego, S. *Projekt budowlano-wykonawczy. Budynek audytoryjny kompleksu obiektów ATR w Fordonie*; Biuro Projektowo-Badawcze Budownictwa Ogólnego Miastoprojekt-Bydgoszcz: Bydgoszcz, Poland, 1999. (In Polish)
53. Zawalski, A. *Ekspertyza ustalająca przyczyny uszkodzeń budynku Auditorium Novum (wraz z łącznikiem) i osiadań terenu przy al. prof. S. Kaliskiego 7 w Bydgoszczy*; Internal Expertise; Bydgoszcz University of Technology: Bydgoszcz, Poland, 2016.
54. Kumor, M.K. *Iły ekspansywne podłoża budowlanego Bydgoszczy*; Wydawnictwa Uczelniane UTP w Bydgoszczy: Bydgoszcz, Poland, 2016; p. 235.

55. Przystański, J. (Ed.) *Posadowienie budowli na gruntach ekspansywnych*; Rozprawy nr 244; Wydawnictwo Politechniki Poznańskiej: Poznań, Poland, 1991; p. 87.
56. Topoliński, S.M.; Gorączko, A.; Sztubecki, J.C.; Bujarkiewicz, A. Monitoring przemieszczeń pionowych słupów obiektu posadowionego na podłożu ekspansywnym. *Czas. Inżynierii Lądowej Środowiska I Archit.* **2017**, *64*, 375–385. [CrossRef]
57. Topoliński, S.M.; Gorączko, A.; Sztubecki, J.C.; Bujarkiewicz, A. The displacement of structures founded on expansive soils-unapparent causes. *E3S Web Conf.* **2018**, *45*, 00098. [CrossRef]
58. Burge, J.H.; Su, P.; Zhao, C.; Zobrist, T. Use of a commercial laser tracker for optical alignment. Optical System Alignment and Tolerancing. In Proceedings of the SPIE-The International Society for Optical Engineering, San Diego, CA, USA, 26–30 August 2007; Volume 6676. [CrossRef]
59. Hexagon_MI_Leica_TDRA6000_Brochure_EN.pdf. Available online: https://www.hexagonmi.com (accessed on 31 May 2022).
60. Wyszkowska, P.; Duchnowski, R. Processing TLS heterogeneous data by applying robust Msplit estimation. *Measurement* **2022**, *197*, 111298. [CrossRef]
61. Wiśniewski, Z. *Rachunek wyrównawczy w geodezji*; Wydawnictwo Uniwersytetu Warmińsko-Mazurskiego w Olsztynie: Olsztyn, Poland, 2016.
62. Zienkiewicz, M. Deformation Analysis of Geodetic Networks by Applying Msplit Estimation with Conditions Binding the Competitive Parameters. *J. Surv. Eng.* **2019**, *145*, 04019001. [CrossRef]
63. Zeidan, Z.; Beshr, A.A.A.; Sameh, S. Structural damage detection of elevated circular water tank and its supporting system using geodetic techniques. *Geod. Cartogr.* **2020**, *69*, 117–140. [CrossRef]
64. SHM-X-Rysomierz.pdf. Available online: https://www.shmsystem.pl/ (accessed on 21 January 2022).
65. Pomiar-ekspercki-v5.4.xlsx. Available online: https://www.shmsystem.pl/wp-content/uploads/2021/03/Pomiar-ekspercki-v5.4.xlsx (accessed on 21 January 2022).
66. Dybeł, K.; Kampczyk, A. Interaction of Colours and Temperatures in Rail Transportation Engineering. In *Proceedings of VIAC 2022 in Budapest*; Chapter: IAC202202005; Czech Institute of Academic Education: Prague, Czech Republic, 2022.
67. Collilieux, X.; Courde, C.; Fruneau, B.; Aimar, M.; Schmidt, G.; Delprat, I.; Defresne, M.A.; Pesce, D.; Bergerault, F.; Wöppelmann, G. Validation of a Corner Reflector installation at Côte d'Azur multi-technique geodetic Observatory. *Adv. Space Res.* **2022**, *70*, 360–370. [CrossRef]
68. Pan, Y.; Ding, H.; Li, J.; Shum, C.K.; Mallick, R.; Jiao, J.; Li, M.; Zhang, Y. Transient hydrology-induced elastic deformation and land subsidence in Australia constrained by contemporary geodetic measurements. *Earth Planet. Sci. Lett.* **2022**, *58*, 117556. [CrossRef]